

Flat Chern Band From Twisted Bilayer MnBi_2Te_4

Biao Lian,^{1,*} Zhaochen Liu,² Yuanbo Zhang,^{2,3} and Jing Wang^{2,3,†}

¹*Princeton Center for Theoretical Science, Princeton University, Princeton, New Jersey 08544, USA*

²*State Key Laboratory of Surface Physics, Department of Physics, Fudan University, Shanghai 200433, China*

³*Institute for Nanoelectronic Devices and Quantum Computing, Fudan University, Shanghai 200433, China*

(Dated: February 17, 2023)

We construct a continuum model for the Moiré superlattice of twisted bilayer MnBi_2Te_4 , and study the band structure of the bilayer in both ferromagnetic (FM) and antiferromagnetic (AFM) phases. We find the system exhibits highly tunable Chern bands with Chern number up to 3. We show that a twist angle of 1° turns the highest valence band into a flat band with Chern number ± 1 that is isolated from all other bands in both FM and AFM phases. This result provides a promising platform for realizing time-reversal breaking correlated topological phases, such as fractional Chern insulator and $p + ip$ topological superconductor. In addition, our calculation indicates that the twisted stacking facilitates the emergence of quantum anomalous Hall effect in MnBi_2Te_4 .

Topology has become one of the central topics in condensed matter physics. The discovery of topological insulator (TI) [1–11], quantum anomalous Hall (QAH) effect [12–18] and other topological states have significantly enriched the variety of quantum matter, and may lead to potential applications in electronics and quantum computation [19–23]. Electron-electron interaction plays an essential role in fractional quantum Hall effect, and there have been proposals of strongly correlated topological states such as fractional TI and fractional Chern insulator (FCI) without magnetic field [24–31]. Experimentally realizing such states is, however, challenging because flat topological electronic bands are generally required for electron-electron interactions to manifest.

Recently, it is shown that Moiré superlattices in twisted or lattice mismatched two-dimensional (2D) materials can give rise to flat topological bands. A prime example is twisted bilayer graphene (tBLG) [32–35], where the lowest two bands carry a fragile topology [36–40] and become flat near the magic twist angle $\theta \approx 1.1^\circ$. In addition, flat valley Chern bands can be realized in tBLG with aligned hBN substrate [41–43], twisted double bilayer graphene [44–46], ABC trilayer graphene on hBN [47–49] and twisted bilayer transition metal dichalcogenides [50, 51], etc. The small bandwidths make electron-electron interactions important [52–59], and further lead to intriguing interacting phases in experiments including superconductivity, correlated insulator and QAH effect.

So far, all of the experimental Moiré systems are time-reversal (TR) invariant at the single particle level, thus the total Chern number always equals to zero. Therefore, even with flat bands, it is difficult to achieve TR breaking interacting topological states such as the FCI in these systems. This motivates us to consider the Moiré superlattice of TR breaking layered materials. A promising system is 3D antiferromagnetic (AFM) topological axion insulator MnBi_2Te_4 [60–78], which can be driven into a ferromagnetic (FM) Weyl semimetal or 3D QAH insulator. The material consists of Van der Waals coupled

septuple layers (SLs) and is FM within each SL. Few-SL MnBi_2Te_4 films have been shown to host intrinsic QAH effects [68].

In this letter, we study the band structure of twisted bi-SL MnBi_2Te_4 (tBMBT) Moiré superlattice as an example of TR breaking Moiré systems. The magnetization of the two SLs may be either the same (FM) or opposite (AFM), both of which are explored here. We find the band structure contains a number of nondegenerate Chern bands, which undergo Chern number topological phase transitions with respect to tunable system parameters such as the twist angle, staggered layer potential and the magnetization. In particular, by tuning staggered layer potential, one can drive the first valence band of both FM and AFM tBMBT into a flat Chern band with Chern number ± 1 around twist angle 1° , which is energetically separated from the other bands. tBMBT thus provides an ideal platform for searching for FCI and other TR breaking interacting topological phases. In addition, low energy bands with Chern number higher than ± 1 may also be realized by tuning the parameters.

The bulk MnBi_2Te_4 has a layered rhombohedral crystal structure with the space group D_{3d}^5 (No. 166). Each unit cell consist of seven-atom layers (Te-Bi-Te-Mn-Te-Bi-Te) arranged along the trigonal z -axis with the ABC-type stacking, referred to as an SL, as shown in Fig. 1(a). The in-plane triangular lattice constant is $a_0 = 4.334 \text{ \AA}$, and the thickness of a unit cell (consisting of 3 SLs) is $c_0 = 40.91 \text{ \AA}$. Neighboring SLs have van der Waals couplings, and the adjacent atomic layers of neighboring SLs form AB stacking in the ground state crystal structure.

Below a Néel temperature of $\sim 25 \text{ K}$, each SL of the bulk MnBi_2Te_4 develops an intralayer FM order on the Mn atoms with an out-of-plane easy axis, but adjacent SLs couple anti-parallel to each other, yielding a topological axion insulator with an out-of-plane layered AFM order. The FM phase with an out-of-plane easy axis is a competing ground state with a slightly higher energy, where the system is a Weyl semimetal or a 3D QAH insulator [60, 61]. The intrinsic magnetism and band inver-

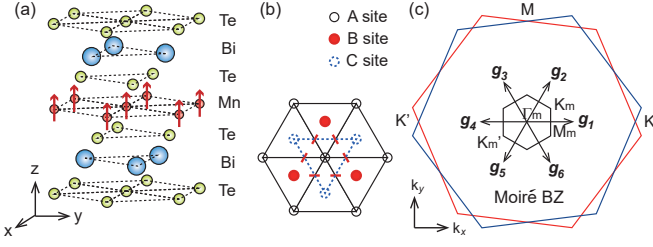


FIG. 1. (a) A single SL of MnBi_2Te_4 , where seven atomic layers form the ABC-type stacking. (b) Top view illustration of A, B, and C stacking configurations of the triangular atomic lattices. (c) The relatively twisted single SL BZ and the Moiré BZ of tBMBT.

sion make it highly promising to realize the intrinsic QAH effect in few-SL MnBi_2Te_4 thin films [60, 61, 64, 68–70].

The weak Van der Waals coupling between SLs allows the implementation of tBMBT by stacking two mono-SLs with a twist angle. The first-principles calculations show that few-SL MnBi_2Te_4 have competing FM and AFM ground states [60, 61, 64]. While the AFM phase is more likely, it may be flipped into FM by a 2 ~ 4T magnetic field [63, 68, 79] or top/bottom FM heterostructure proximities. Therefore, we investigate both the FM and AFM phases of tBMBT, where the two SLs have the same and opposite z direction FM orders, respectively.

Model. We now construct an effective continuum model [32] for tBMBT formed by two SLs stacked on top of each other with a twist angle θ , which is generic for C_{3z} symmetric layered magnetic materials with low energy Dirac electrons. The Hamiltonian for such a model can be written in real space as

$$H = \begin{pmatrix} h_{l, \pm \frac{\theta}{2}}(-i\nabla) + U_d & T(\mathbf{r}) \\ T^\dagger(\mathbf{r}) & h_{l, -\frac{\theta}{2}}(-i\nabla) - U_d \end{pmatrix}, \quad (1)$$

where $-i\nabla$ is the 2D momentum in the monolayer Brillouin zone (BZ) of each SL, $h_{l, \pm \frac{\theta}{2}}$ is the 4×4 monolayer Hamiltonian of the l -th SL ($l = 1, 2$) rotated by angle $\pm\theta/2$, U_d is a staggered layer potential which can be tuned by the top and back gates, and $T(\mathbf{r})$ is the 4×4 interlayer Moiré hopping potential. The basis of the monolayer Hamiltonian $h_{l, \pm \frac{\theta}{2}}$ is $(|p_{z, \text{Bi}}^+, \uparrow\rangle, |p_{z, \text{Te}}^-, \downarrow\rangle, |p_{z, \text{Te}}^-, \uparrow\rangle, |p_{z, \text{Bi}}^+, \downarrow\rangle)^T$ of the l -th SL ($l = 1, 2$), where superscripts “+”, “-” stand for parity. $|p_{z, \text{Bi}}^+, s\rangle$ is the spin s bonding state of the p_z orbitals of two Bi layers, and $|p_{z, \text{Te}}^-, s\rangle$ is the spin s antibonding state of the two p_z orbitals of the top and bottom Te layers. Since the low energy physics in MnBi_2Te_4 is located near the Γ point, we set the origin of the momentum $-i\nabla$ to be Γ of the monolayer BZ. In the below, we study the FM and AFM phases separately.

FM phase. Depending on the strength of FM exchange field, the untwisted FM bilayer MnBi_2Te_4 may be either a QAH insulator of Chern number ± 1 , or a trivial insula-

tor which enters the QAH phase under a small magnetic field [68, 69]. To include both possibilities, we introduce a dimensionless FM strength tuning parameter γ_f , where we fix $|\gamma_f| = 1$ to be the critical FM order strength above (below) which the untwisted FM bilayer MnBi_2Te_4 is a QAH (trivial) insulator [79]. Experimentally, γ_f is tunable by the magnetic field.

The monolayer Hamiltonian in Eq. (1) for a FM tBMBT with FM strength γ_f can be written as

$$h_{l, \pm \frac{\theta}{2}}(\mathbf{k}) = R_{\pm \frac{\theta}{2}}^\dagger [h_N(\mathbf{k}) + \gamma_f h_{\text{FM}}(\mathbf{k})] R_{\pm \frac{\theta}{2}}, \quad (2)$$

where $\mathbf{k} = (k_x, k_y)$ is the 2D electron momentum, $R_{\pm \frac{\theta}{2}} = \text{diag}(e^{\pm i\theta/4}, e^{\mp i\theta/4}, e^{\mp i\theta/4}, e^{\pm i\theta/4})$ is the angle $\pm\theta/2$ rotation matrix about the z axis. $h_N(\mathbf{k})$ and $h_{\text{FM}}(\mathbf{k})$ are the nonmagnetic part and FM part of the $\mathbf{k} \cdot \mathbf{p}$ Hamiltonian of single SL MnBi_2Te_4 at the Γ point, respectively, which take the forms

$$h_N(\mathbf{k}) = \epsilon_0(\mathbf{k}) + \begin{pmatrix} m(\mathbf{k}) & \alpha k_- \\ \alpha k_+ & -m(\mathbf{k}) \\ & -m(\mathbf{k}) & \alpha k_- \\ & \alpha k_+ & m(\mathbf{k}) \end{pmatrix}, \quad (3)$$

and

$$h_{\text{FM}}(\mathbf{k}) = \begin{pmatrix} m_1(\mathbf{k}) & \alpha' k_- \\ \alpha' k_+ & -m_2(\mathbf{k}) \\ & m_2(\mathbf{k}) & -\alpha' k_- \\ & -\alpha' k_+ & -m_1(\mathbf{k}) \end{pmatrix}. \quad (4)$$

Here $\epsilon_0(\mathbf{k}) = \gamma \mathbf{k}^2$ is the particle-hole asymmetry term proportional to the identity matrix, $k_{\pm} \equiv k_x \pm ik_y$, $m(\mathbf{k}) = m_0 + \beta_0 \mathbf{k}^2$, and $m_j(\mathbf{k}) = m_j + \beta_j \mathbf{k}^2$ ($j = 1, 2$).

The interlayer Moiré hopping potential $T(\mathbf{r})$ is spatially periodic. To the lowest order, it can be Fourier expanded as

$$T(\mathbf{r}) = T_0 + \sum_{j=1}^6 T_j e^{i\mathbf{g}_j \cdot \mathbf{r}}, \quad (5)$$

where \mathbf{g}_j ($1 \leq j \leq 6$) are the six smallest Moiré reciprocal vectors with length $|\mathbf{g}_j| = 8\pi \sin(\theta/2)/\sqrt{3}a_0$ as shown in Fig. 1(c). $\mathbf{r} = 0$ is defined as an AA stacking center, where the adjacent atomic layers of two SLs form AA stacking. The matrices can be divided into

$$T_j = T_j^N + \gamma_f T_j^{\text{FM}}, \quad (0 \leq j \leq 6) \quad (6)$$

where T_j^N and T_j^{FM} are the nonmagnetic part and FM part, respectively. The form of matrices T_j and the parameters for the FM phase estimated from bulk calculations are given in the Supplementary Material (SM) [79].

We now investigate the Moiré band structure of the FM tBMBT with respect to θ , U_d and γ_f . To distinguish from the original monolayer BZ, we denote the high symmetry points of the hexagonal Moiré BZ as Γ_m , K_m and

M_m . The bands of FM tMBT are generically nondegenerate, many of which carry nonzero Chern numbers. The FM tMBT has C_{3z} and $C_{2x}\mathcal{T}$ symmetries at $U_d = 0$ (\mathcal{T} for TR). A nonzero U_d is odd under $C_{2x}\mathcal{T}$ and thus breaks $C_{2x}\mathcal{T}$. Since the Hall conductance σ_{xy} is invariant under $C_{2x}\mathcal{T}$, the band Chern numbers of FM tMBT are invariant under $U_d \rightarrow -U_d$.

Fig. 2(a)-(e) show typical examples of the FM tMBT Moiré band structures, where the Chern number of the j -th conduction (valence) band is denoted by C_{Cj} (C_{Vj}), and the parameters are given in the caption. The charge neutrality point (CNP) is set as zero. In general, the Chern numbers of the lowest several bands are tunable up to ± 3 . However, most bands except for the first conduction and valence bands have no indirect gaps among each other. Therefore, the system is metallic with nonzero Fermi surface Berry phases at high fillings.

Here we mainly focus on the first conduction and valence bands of the FM phase. In the parameter space of θ , U_d and γ_f , they undergo multiple Chern number topological phase transitions via gap closings at high symmetry points. Fig. 2(f) shows the Chern number phase diagram of the first conduction and valence bands (C_{C1} , C_{V1}) with respect to θ and γ_f at fixed $U_d = 40$ meV. The gap between the first conduction and valence bands closes at Γ_m point around $\gamma_f = 0.93$ for a wide range of θ , which leads to an exchange of Chern number 1 between these two bands. Accordingly, the FM tMBT at the CNP is a QAH insulator with Chern number -1 when $\gamma_f > 0.93$, and the first valence band carries Chern number $C_{V1} = -1$. Therefore, the FM tMBT enters the QAH phase at a smaller FM strength γ_f than the untwisted FM bilayer MnBi_2Te_4 , which suggests that twisting helps achieve the QAH effect in bilayer MnBi_2Te_4 . In addition, the first conduction band undergoes a gap closing with the second conduction band at K_M and K'_M points at angle $\theta \approx 1.2^\circ$ as shown in Fig. 2(f), where its Chern number changes from 0 to 2.

Fig. 2(g) shows the phase diagram with respect to U_d and γ_f at fixed angle $\theta = 1^\circ$. As one can see, adding a staggered layer potential U_d also helps achieve the QAH effect of Chern number -1 at the CNP, and accordingly $C_{V1} = -1$. Besides, the Chern number of the first conduction band changes by 3 at $U_d \approx 10$ meV, which is induced by the gap closing between the first and second conduction bands at three M_m points.

In particular, the first valence band of the FM tMBT with Chern number either -1 or 0 can be made extremely flat, and the band is energetically separated from other bands near twist angle $\theta = 1^\circ$. It is therefore promising to realize TR breaking interacting topological states such as the FCI and the $p + ip$ chiral topological superconductor (TSC). Generally speaking, adding a staggered layer potential U_d flattens the first valence band but not the first conduction band, due to the particle-hole asymmetric term $\epsilon_0(\mathbf{k})$ in Eq. (3). Fig. 2(a) and (b) show the band

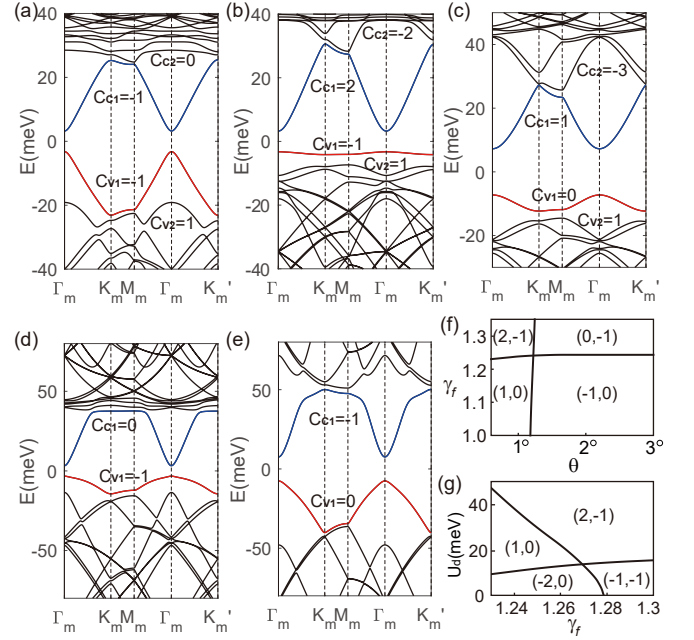


FIG. 2. The band structure of the FM tMBT for (a) $\theta = 1^\circ$, $U_d = 10$ meV, $\gamma_f = 1.02$, (b) $\theta = 1^\circ$, $U_d = 40$ meV, $\gamma_f = 1.02$, (c) $\theta = 1^\circ$, $U_d = 40$ meV, $\gamma_f = 0.75$, (d) $\theta = 2^\circ$, $U_d = 40$ meV, $\gamma_f = 1.02$ and (e) $\theta = 3^\circ$, $U_d = 40$ meV, $\gamma_f = 0.75$. (f) Chern numbers of the first conduction and valence bands (C_{C1} , C_{V1}) as a function of angle θ and exchange field strength γ_f , where $U_d = 40$ meV is set. (g) (C_{C1} , C_{V1}) for $\theta = 1^\circ$ as a function of γ_f and staggered layer potential U_d .

structures at $\theta = 1^\circ$ and $\gamma_f = 1.02$ with $U_d = 10$ meV and 40 meV, respectively, where the first valence band has Chern number $C_{V1} = -1$, and the system has Chern number -1 when the Fermi level is at CNP. In particular, when $U_d = 40$ meV in Fig. 2(b), the bandwidth of the first valence band is suppressed down to $W \approx 1$ meV, while its gap with the other nearest bands is $\Delta \approx 4$ meV. Such an isolated flat Chern band is therefore an ideal platform for realizing the FCI, where the electron filling is readily tuned by a gate. For an estimation, taking the dielectric constant of the MnBi_2Te_4 film $\epsilon_r \approx 10$, one obtains a Coulomb interaction energy $U \approx 6$ meV for filling in the first tMBT band, which easily exceeds the bandwidth and thus makes the FCI possible. Besides, the FM strength γ_f can further tune the Chern number of the first valence band and accordingly the Chern number at CNP. Fig. 2(c) shows the bands at $\theta = 1^\circ$, $\gamma_f = 0.75$ and $U_d = 40$ meV, where both the first valence band and the CNP gap have Chern number 0 . In this case, the first valence band realizes a topologically trivial flat band of bandwidth smaller than 5 meV.

With either Chern number 0 or -1 , the nondegenerate flat valence band allows a single Fermi surface with large density of states when partially filled, leading to a chance of realizing an intrinsic $p + ip$ chiral TSC if a

nodeless pairing is developed [80–83]. The superconductivity experimentally discovered in other Moiré systems suggest that superconductivity is more likely to occur in the presence of Moiré superlattices [84], where one possible mechanism is the Moiré pattern enhances electron-phonon coupling if the superconductivity is phonon induced [85–87]. Therefore, the $p + ip$ TSC might be more achievable in TR breaking Moiré superlattices such as tBMBT here than other TR breaking systems.

When θ is far from 1° , it is difficult to obtain energetically separated flat bands. For smaller θ , the bandwidths are smaller, but there are hardly indirect gaps except for the CNP gap. For larger θ , not only indirect gaps are rare, but also the bands become more dispersive, as shown in the two examples of Fig. 2(d) and 2(e) at $\theta = 2^\circ$ and 3° with $U_d = 40$ meV, respectively. Detailed examination reveals that the optimal angles for flat bands in the FM tBMBT fall within $0.8^\circ \lesssim \theta \lesssim 1.2^\circ$.

AFM phase. The monolayer Hamiltonian of the l -th layer ($l = 1, 2$) in Eq. (1) for the AFM tBMBT takes the form

$$h_{l,\pm\frac{\theta}{2}}(\mathbf{k}) = R_{\pm\frac{\theta}{2}}^\dagger [h_N(\mathbf{k}) - (-1)^l \gamma_{af} h_{AFM}(\mathbf{k})] R_{\pm\frac{\theta}{2}}, \quad (7)$$

where $h_N(\mathbf{k})$ is still given in Eq. (3) but with different parameters from FM phase, and the AFM term is approximated as

$$h_{AFM}(\mathbf{k}) = \text{diag}(m_1, -m_2, m_2, -m_1), \quad (8)$$

which has no \mathbf{k} dependence. γ_{af} tunes the AFM order strength ($\gamma_{af} = 1$ represents the strength estimated from the first-principles calculations). The interlayer Moiré potential only contains the nonmagnetic part of Eq. (6), i.e., $T_j = T_j^N$. The matrices T_j and the parameters for the AFM phase are listed in the SM [79]. In contrast to the 3D AFM MnBi_2Te_4 which has two-fold degenerate bands protected by the \mathcal{PT} symmetry (\mathcal{P} for inversion), the AFM tBMBT has nondegenerate bands, since the twist angle breaks the \mathcal{PT} symmetry. It only has C_{3z} and C_{2x} symmetries at $U_d = 0$, and C_{2x} is further broken when U_d is nonzero.

Since σ_{xy} is odd under C_{2x} , all the bands of the AFM tBMBT have Chern number zero at $U_d = 0$. Nonzero Chern numbers can only arise at nonzero U_d , and are odd under $U_d \rightarrow -U_d$. Fig. 3(a) and 3(b) show the band structure of AFM tBMBT at $\theta = 1^\circ$, $\gamma_{af} = 1$ for $U_d = 10$ meV and 40 meV, respectively. Similar to the FM phase, increasing U_d flattens the first valence band but not the first conduction band. Besides, the Chern number of the first valence band undergoes a transition from 0 to 1 as U_d increases, which is induced by the gap closing at K'_m point (note that K_m and K'_m are not symmetric). Fig. 3(d) shows the Chern number phase diagram of the first conduction and valence bands with respect to θ and U_d . Therefore, the first valence band of the AFM tBMBT can also be driven into a flat Chern band

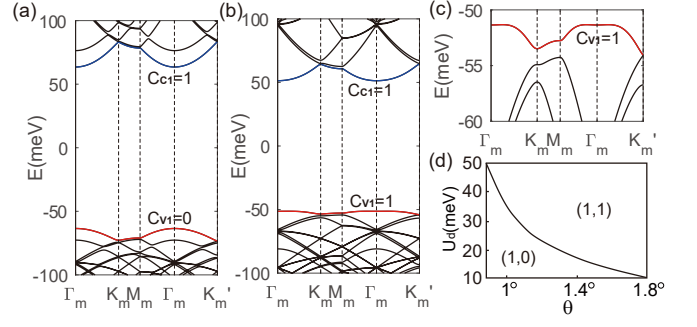


FIG. 3. The band structure of the AFM tBMBT for (a) $\theta = 1^\circ$, $\gamma_{af} = 1$, $U_d = 10$ meV, and (b) $\theta = 1^\circ$, $\gamma_{af} = 1$, $U_d = 40$ meV. (c) Zoom-in plot of the valence band structure in (b), showing the bandwidth of the first valence band. (d) (C_{C1}, C_{V1}) as a function of the twist angle θ and the staggered layer potential U_d .

separated from the other bands. Fig. 3(c) shows a zoom-in plot of Fig. 3(b), where the first valence band has a small bandwidth around $W \approx 3$ meV, but with a smaller gap to second valence band. The CNP gap always has Chern number 0. The conclusions are qualitatively insensitive to γ_{af} . This allows the realization of the QAH effect with Chern number ± 1 in the AFM tBMBT by fully emptying the first valence band. More importantly, this indicates it is also possible to realize FCI and other interacting topological phases in the AFM tBMBT. Again, we find the optimal angle for realizing energetically isolated flat bands in AFM tBMBT is around $\theta = 1^\circ$. It is worth mentioning that a larger θ can lead to relatively flat first valence band with $C_{V1} = -2$ but without indirect gap to higher bands [79].

Discussion. The tBMBT with a twist angle near 1° host isolated Moiré Chern bands, whose bandwidth is significantly smaller than the Coulomb repulsion energy ($2 \lesssim U/W \lesssim 6$). Mechanically robust single SL of MnBi_2Te_4 has been obtained experimentally [68], making it possible to implement tBMBT. The broad variety of tuning parameters including twist angle, staggered layer potential, electron filling, magnetic field, and hydrostatic pressure makes tBMBT a promising platform for realizing the correlated topological phases. The FM phase is more favored than the AFM phase for the flat Chern band to have a larger gap to other bands. Disorders also inevitably exist in realistic materials. Short range scatters will broaden the bandwidth, and thus reduce U/W , but the correlated topological phases should be robust against long-range potential fluctuations (i.e. charge puddles).

tBMBT may provide the first experimental platform for isolated Moiré flat Chern bands. Besides tBMBT, there are rich choices of magnetic layered topological materials such as $\text{Mn}_2\text{Bi}_2\text{Te}_5$ [88] and MnBi_4Te_7 [89], etc. These materials provide fertile playground for investigat-

ing emergent correlated topological states in twisted multilayers with tunable U/W .

Acknowledgments. B.L. is supported by Princeton Center for Theoretical Science at Princeton University. Y.Z. acknowledges support from National Key Research Program of China (grant nos. 2016YFA0300703, 2018YFA0305600), NSF of China (grant nos. U1732274, 11527805, 11425415 and 11421404), and Strategic Priority Research Program of Chinese Academy of Sciences (grant no. XDB30000000). J.W. is supported by the Natural Science Foundation of China through Grant No. 11774065, the National Key Research Program of China under Grant No. 2016YFA0300703, the Natural Science Foundation of Shanghai under Grant Nos. 17ZR1442500, 19ZR1471400.

* biao@princeton.edu

† wjingphys@fudan.edu.cn

- [1] C. L. Kane and E. J. Mele, “ Z_2 topological order and the quantum spin hall effect,” *Phys. Rev. Lett.* **95**, 146802 (2005).
- [2] C. L. Kane and E. J. Mele, “Quantum spin hall effect in graphene,” *Phys. Rev. Lett.* **95**, 226801 (2005).
- [3] B. A. Bernevig, T. L. Hughes, and S.-C. Zhang, “Quantum spin hall effect and topological phase transition in hgte quantum wells,” *Science* **314**, 1757–1761 (2006).
- [4] M. König, S. Wiedmann, C. Brüne, A. Roth, H. Buhmann, L. W. Molenkamp, X.-L. Qi, and S.-C. Zhang, “Quantum spin hall insulator state in hgte quantum wells,” *Science* **318**, 766–770 (2007).
- [5] L. Fu, C. L. Kane, and E. J. Mele, “Topological insulators in three dimensions,” *Phys. Rev. Lett.* **98**, 106803 (2007).
- [6] Y. L. Chen, J. G. Analytis, J.-H. Chu, Z. K. Liu, S.-K. Mo, X. L. Qi, H. J. Zhang, D. H. Lu, X. Dai, Z. Fang, S. C. Zhang, I. R. Fisher, Z. Hussain, and Z.-X. Shen, “Experimental realization of a three-dimensional topological insulator, Bi_2Te_3 ,” *Science* **325**, 178–181 (2009).
- [7] H. Zhang, C.-X. Liu, X.-L. Qi, X. Dai, Z. Fang, and S.-C. Zhang, “Topological insulators in Bi_2Se_3 , Bi_2Te_3 and Sb_2Te_3 with a single dirac cone on the surface,” *Nature Phys.* **5**, 438–442 (2009).
- [8] Y. Xia, D. Qian, D. Hsieh, L. Wray, A. Pal, H. Lin, A. Bansil, D. Grauer, Y. S. Hor, R. J. Cava, and M. Z. Hasan, “Observation of a large-gap topological-insulator class with a single dirac cone on the surface,” *Nature Phys.* **5**, 398–402 (2009).
- [9] M. Z. Hasan and C. L. Kane, “Colloquium: Topological insulators,” *Rev. Mod. Phys.* **82**, 3045–3067 (2010).
- [10] X.-L. Qi and S.-C. Zhang, “Topological insulators and superconductors,” *Rev. Mod. Phys.* **83**, 1057–1110 (2011).
- [11] J. Wang and S.-C. Zhang, “Topological states of condensed matter,” *Nature Mat.* **16**, 1062–1067 (2017).
- [12] F. D. M. Haldane, “Model for a quantum hall effect without landau levels: Condensed-matter realization of the “parity anomaly”,” *Phys. Rev. Lett.* **61**, 2015–2018 (1988).
- [13] C.-X. Liu, X.-L. Qi, X. Dai, Z. Fang, and S.-C. Zhang, “Quantum anomalous hall effect in $\text{Hg}_{1-y}\text{Mn}_y\text{Te}$ quantum wells,” *Phys. Rev. Lett.* **101**, 146802 (2008).
- [14] R. Yu, W. Zhang, H.-J. Zhang, S.-C. Zhang, X. Dai, and Z. Fang, “Quantized anomalous hall effect in magnetic topological insulators,” *Science* **329**, 61–64 (2010).
- [15] C.-Z. Chang, J. Zhang, X. Feng, J. Shen, Z. Zhang, M. Guo, K. Li, Y. Ou, P. Wei, L.-L. Wang, Z.-Q. Ji, Y. Feng, S. Ji, X. Chen, J. Jia, X. Dai, Z. Fang, S.-C. Zhang, K. He, Y. Wang, L. Lu, X.-C. Ma, and Q.-K. Xue, “Experimental observation of the quantum anomalous hall effect in a magnetic topological insulator,” *Science* **340**, 167–170 (2013).
- [16] J. Wang, B. Lian, H. Zhang, Y. Xu, and S.-C. Zhang, “Quantum anomalous hall effect with higher plateaus,” *Phys. Rev. Lett.* **111**, 136801 (2013).
- [17] J. Wang, B. Lian, and S.-C. Zhang, “Quantum anomalous hall effect in magnetic topological insulators,” *Phys. Scr.* **T164**, 014003 (2015).
- [18] C.-X. Liu, S.-C. Zhang, and X.-L. Qi, “The quantum anomalous hall effect: Theory and experiment,” *Annu. Rev. Condens. Mat. Phys.* **7**, 301–321 (2016).
- [19] D. A. Ivanov, “Non-abelian statistics of half-quantum vortices in p -wave superconductors,” *Phys. Rev. Lett.* **86**, 268–271 (2001).
- [20] A. Yu. Kitaev, “Fault-tolerant quantum computation by anyons,” *Ann. Phys.* **303**, 2–30 (2003).
- [21] C. Nayak, S. H. Simon, A. Stern, M. Freedman, and S. Das Sarma, “Non-abelian anyons and topological quantum computation,” *Rev. Mod. Phys.* **80**, 1083–1159 (2008).
- [22] J. Alicea, Y. Oreg, G. Refael, F. von Oppen, and M. P. A. Fisher, “Non-abelian statistics and topological quantum information processing in 1d wire networks,” *Nature Phys.* **7**, 412–417 (2011).
- [23] B. Lian, X.-Q. Sun, A. Vaezi, X.-L. Qi, and S.-C. Zhang, “Topological quantum computation based on chiral majorana fermions,” *Proc. Natl. Acad. Sci. U.S.A.* **115**, 10938–10942 (2018).
- [24] M. Levin and A. Stern, “Fractional topological insulators,” *Phys. Rev. Lett.* **103**, 196803 (2009).
- [25] J. Maciejko, X.-L. Qi, A. Karch, and S.-C. Zhang, “Fractional topological insulators in three dimensions,” *Phys. Rev. Lett.* **105**, 246809 (2010).
- [26] X.-L. Qi, “Generic wave-function description of fractional quantum anomalous hall states and fractional topological insulators,” *Phys. Rev. Lett.* **107**, 126803 (2011).
- [27] E. Tang, J.-W. Mei, and X.-G. Wen, “High-temperature fractional quantum hall states,” *Phys. Rev. Lett.* **106**, 236802 (2011).
- [28] K. Sun, Z. Gu, H. Katsura, and S. Das Sarma, “Nearly flatbands with nontrivial topology,” *Phys. Rev. Lett.* **106**, 236803 (2011).
- [29] T. Neupert, L. Santos, C. Chamon, and C. Mudry, “Fractional quantum hall states at zero magnetic field,” *Phys. Rev. Lett.* **106**, 236804 (2011).
- [30] A. Stern, “Fractional topological insulators: A pedagogical review,” *Ann. Rev. Condens. Mat. Phys.* **7**, 349–368 (2016).
- [31] E. M. Spanton, A. A. Zibrov, H. Zhou, T. Taniguchi, K. Watanabe, M. P. Zaletel, and A. F. Young, “Observation of fractional chern insulators in a van der waals heterostructure,” *Science* **360**, 62–66 (2018).
- [32] R. Bistritzer and A. H. MacDonald, “Moiré bands in twisted double-layer graphene,” *Proc. Natl. Acad. Sci.*

- U.S.A. **108**, 12233–12237 (2011).
- [33] Y. Cao, V. Fatemi, S. Fang, K. Watanabe, T. Taniguchi, E. Kaxiras, and P. Jarillo-Herrero, “Unconventional superconductivity in magic-angle graphene superlattices,” *Nature* **556**, 43 (2018).
 - [34] M. Yankowitz, S. Chen, H. Polshyn, Y. Zhang, K. Watanabe, T. Taniguchi, D. Graf, A. F. Young, and C. R. Dean, “Tuning superconductivity in twisted bilayer graphene,” *Science* **363**, 1059–1064 (2019).
 - [35] X. Lu, P. Stepanov, W. Yang, M. Xie, M. A. Aamir, I. Das, C. Urgell, K. Watanabe, T. Taniguchi, G. Zhang, A. Bachtold, A. H. MacDonald, and D. K. Efetov, “Superconductors, Orbital Magnets, and Correlated States in Magic Angle Bilayer Graphene,” arXiv e-prints, arXiv:1903.06513 (2019), [arXiv:1903.06513 \[cond-mat.mes-hall\]](#).
 - [36] Z. Song, Z. Wang, W. Shi, G. Li, C. Fang, and B. A. Bernevig, “All magic angles in twisted bilayer graphene are topological,” *Phys. Rev. Lett.* **123**, 036401 (2019).
 - [37] H. C. Po, L. Zou, T. Senthil, and A. Vishwanath, “Faithful tight-binding models and fragile topology of magic-angle bilayer graphene,” *Phys. Rev. B* **99**, 195455 (2019).
 - [38] J. Ahn, S. Park, and B.-J. Yang, “Failure of nielsen-ninomiya theorem and fragile topology in two-dimensional systems with space-time inversion symmetry: Application to twisted bilayer graphene at magic angle,” *Phys. Rev. X* **9**, 021013 (2019).
 - [39] B. Lian, F. Xie, and B. A. Bernevig, “The Landau Level of Fragile Topology,” arXiv e-prints, arXiv:1811.11786 (2018), [arXiv:1811.11786 \[cond-mat.mes-hall\]](#).
 - [40] F. Xie, Z. Song, B. Lian, and B. A. Bernevig, “Topology-Bounded Superfluid Weight In Twisted Bilayer Graphene,” arXiv e-prints, arXiv:1906.02213 (2019), [arXiv:1906.02213 \[cond-mat.supr-con\]](#).
 - [41] N. Bultinck, S. Chatterjee, and M. P. Zaletel, “Anomalous Hall ferromagnetism in twisted bilayer graphene,” arXiv e-prints, arXiv:1901.08110 (2019), [arXiv:1901.08110 \[cond-mat.str-el\]](#).
 - [42] A. L. Sharpe, E. J. Fox, A. W. Barnard, J. Finney, K. Watanabe, T. Taniguchi, M. A. Kastner, and D. Goldhaber-Gordon, “Emergent ferromagnetism near three-quarters filling in twisted bilayer graphene,” *Science* (2019), [10.1126/science.aaw3780](#).
 - [43] M. Serlin, C. L. Tschirhart, H. Polshyn, Y. Zhang, J. Zhu, K. Watanabe, T. Taniguchi, L. Balents, and A. F. Young, “Intrinsic quantized anomalous Hall effect in a moiré heterostructure,” arXiv e-prints, arXiv:1907.00261 (2019), [arXiv:1907.00261 \[cond-mat.str-el\]](#).
 - [44] X. Liu, Z. Hao, E. Khalaf, J. Y. Lee, K. Watanabe, T. Taniguchi, A. Vishwanath, and P. Kim, “Spin-polarized Correlated Insulator and Superconductor in Twisted Double Bilayer Graphene,” arXiv e-prints, arXiv:1903.08130 (2019), [arXiv:1903.08130 \[cond-mat.mes-hall\]](#).
 - [45] Y. Cao, D. Rodan-Legrain, O. Rubies-Bigordà, J. M. Park, K. Watanabe, T. Taniguchi, and P. Jarillo-Herrero, “Electric Field Tunable Correlated States and Magnetic Phase Transitions in Twisted Bilayer-Bilayer Graphene,” arXiv e-prints, arXiv:1903.08596 (2019), [arXiv:1903.08596 \[cond-mat.str-el\]](#).
 - [46] C. Shen, N. Li, S. Wang, Y. Zhao, J. Tang, J. Liu, J. Tian, Y. Chu, K. Watanabe, T. Taniguchi, R. Yang, Z. Y. Meng, D. Shi, and G. Zhang, “Observation of superconductivity with Tc onset at 12K in electrically tunable twisted double bilayer graphene,” arXiv e-prints, arXiv:1903.06952 (2019), [arXiv:1903.06952 \[cond-mat.supr-con\]](#).
 - [47] Y.-H. Zhang, D. Mao, Y. Cao, P. Jarillo-Herrero, and T. Senthil, “Nearly flat chern bands in moiré superlattices,” *Phys. Rev. B* **99**, 075127 (2019).
 - [48] G. Chen, L. Jiang, S. Wu, B. Lyu, H. Li, B. L. Chittari, K. Watanabe, T. Taniguchi, Z. Shi, J. Jung, Y. Zhang, and F. Wang, “Evidence of a gate-tunable mott insulator in a trilayer graphene moiré superlattice,” *Nature Phys.* **15**, 237 (2019).
 - [49] G. Chen, A. L. Sharpe, P. Gallagher, I. T. Rosen, E. J. Fox, L. Jiang, B. Lyu, H. Li, K. Watanabe, T. Taniguchi, J. Jung, Z. Shi, D. Goldhaber-Gordon, Y. Zhang, and F. Wang, “Signatures of tunable superconductivity in a trilayer graphene moiré superlattice,” *Nature* (2019), [10.1038/s41586-019-1393-y](#).
 - [50] F. Wu, T. Lovorn, E. Tutuc, I. Martin, and A. H. MacDonald, “Topological insulators in twisted transition metal dichalcogenide homobilayers,” *Phys. Rev. Lett.* **122**, 086402 (2019).
 - [51] C. Jin, E. C. Regan, A. Yan, M. Iqbal Bakti Utama, D. Wang, S. Zhao, Y. Qin, S. Yang, Z. Zheng, S. Shi, K. Watanabe, T. Taniguchi, S. Tongay, A. Zettl, and F. Wang, “Observation of moiré excitons in wse₂/ws₂ heterostructure superlattices,” *Nature* **567**, 76 (2019).
 - [52] J. Kang and O. Vafek, “Strong coupling phases of partially filled twisted bilayer graphene narrow bands,” *Phys. Rev. Lett.* **122**, 246401 (2019).
 - [53] M. Koshino, N. F. Q. Yuan, T. Koretsune, M. Ochi, K. Kuroki, and L. Fu, “Maximally localized wannier orbitals and the extended hubbard model for twisted bilayer graphene,” *Phys. Rev. X* **8**, 031087 (2018).
 - [54] H.C. Po, L. Zou, A. Vishwanath, and T. Senthil, “Origin of mott insulating behavior and superconductivity in twisted bilayer graphene,” *Phys. Rev. X* **8**, 031089 (2018).
 - [55] J. F. Dodaro, S. A. Kivelson, Y. Schattner, X. Q. Sun, and C. Wang, “Phases of a phenomenological model of twisted bilayer graphene,” *Phys. Rev. B* **98**, 075154 (2018).
 - [56] Y. Xie, B. Lian, B. Jäck, X. Liu, C.-L. Chiu, K. Watanabe, T. Taniguchi, B. A. Bernevig, and A. Yazdani, “Spectroscopic signatures of many-body correlations in magic-angle twisted bilayer graphene,” *Nature* (2019), [10.1038/s41586-019-1422-x](#).
 - [57] A. Kerelsky, L. J. McGilly, D. M. Kennes, L. Xian, M. Yankowitz, S. Chen, K. Watanabe, T. Taniguchi, J. Hone, C. Dean, A. Rubio, and A. N. Pasupathy, “Maximized electron interactions at the magic angle in twisted bilayer graphene,” *Nature* (2019), [10.1038/s41586-019-1431-9](#).
 - [58] Y. Choi, J. Kemmer, Y. Peng, A. Thomson, H. Arora, R. Polski, Y. Zhang, H. Ren, J. Alicea, G. Refael, F. von Oppen, K. Watanabe, T. Taniguchi, and S. Nadj-Perge, “Imaging Electronic Correlations in Twisted Bilayer Graphene near the Magic Angle,” arXiv e-prints, arXiv:1901.02997 (2019), [arXiv:1901.02997 \[cond-mat.mes-hall\]](#).
 - [59] Y. Jiang, X. Lai, K. Watanabe, T. Taniguchi, K. Haule, J. Mao, and E.Y. Andrei, “Charge-order and broken rotational symmetry in magic angle twisted bilayer graphene,” *Nature* (2019), [10.1038/s41586-019-1460-4](#).

- [60] D. Zhang, M. Shi, T. Zhu, D. Xing, H. Zhang, and J. Wang, “Topological axion states in the magnetic insulator mnbi_2te_4 with the quantized magnetoelectric effect,” *Phys. Rev. Lett.* **122**, 206401 (2019).
- [61] J. Li, Y. Li, S. Du, Z. Wang, B.-L. Gu, S.-C. Zhang, K. He, W. Duan, and Y. Xu, “Intrinsic magnetic topological insulators in van der waals layered mnbi_2te_4 -family materials,” *Sci. Adv.* **5**, eaaw5685 (2019).
- [62] Y. Gong, J. Guo, J. Li, K. Zhu, M. Liao, X. Liu, Q. Zhang, L. Gu, L. Tang, X. Feng, D. Zhang, W. Li, C. Song, L. Wang, P. Yu, X. Chen, Y. Wang, H. Yao, W. Duan, Y. Xu, S.-C. Zhang, X. Ma, Q.-K. Xue, and K. He, “Experimental realization of an intrinsic magnetic topological insulator,” *Chin. Phys. Lett.* **36**, 076801 (2019).
- [63] M. M. Otrokov, I. I. Klimovskikh, H. Bentmann, A. Zeugner, Z. S. Aliev, S. Gass, Anja U. B. Wolter, A. V. Koroleva, D. Estyunin, A. M. Shikin, M. Blanco-Rey, M. Hoffmann, A. Yu. Vyazovskaya, S. V. Ereemeev, Y. M. Koroteev, I. R. Amiraslanov, M. B. Babanly, N. T. Mamedov, N. A. Abdullayev, V. N. Zverev, B. Büchner, E. F. Schwier, S. Kumar, A. Kimura, L. Petaccia, G. Di Santo, R. C. Vidal, S. Schatz, K. Kißner, C.-H. Min, S. K. Moser, T. R. F. Peixoto, F. Reinert, A. Ernst, P. M. Echenique, A. Isaeva, and E. V. Chulkov, “Prediction and observation of the first antiferromagnetic topological insulator,” arXiv e-prints , arXiv:1809.07389 (2018), [arXiv:1809.07389 \[cond-mat.mtrl-sci\]](#).
- [64] M. M. Otrokov, I. P. Rusinov, M. Blanco-Rey, M. Hoffmann, A. Yu. Vyazovskaya, S. V. Ereemeev, A. Ernst, P. M. Echenique, A. Arnau, and E. V. Chulkov, “Unique thickness-dependent properties of the van der waals interlayer antiferromagnet mnbi_2te_4 films,” *Phys. Rev. Lett.* **122**, 107202 (2019).
- [65] S. Huat Lee, Y. Zhu, Y. Wang, L. Miao, T. Pillsbury, S. Kempinger, D. Graf, N. Alem, C.-Z. Chang, N. Samarth, and Z. Mao, “Spin scattering and noncollinear spin structure-induced intrinsic anomalous Hall effect in antiferromagnetic topological insulator MnBi_2Te_4 ,” arXiv e-prints , arXiv:1812.00339 (2018), [arXiv:1812.00339 \[cond-mat.mtrl-sci\]](#).
- [66] J.-Q. Yan, Q. Zhang, T. Heitmann, Z. Huang, K. Y. Chen, J.-G. Cheng, W. Wu, D. Vaknin, B. C. Sales, and R. J. McQueeney, “Crystal growth and magnetic structure of mnbi_2te_4 ,” *Phys. Rev. Materials* **3**, 064202 (2019).
- [67] B. Chen, F. Fei, D. Zhang, B. Zhang, W. Liu, S. Zhang, P. Wang, B. Wei, Y. Zhang, Z. Zuo, J. Guo, Q. Liu, Z. Wang, X. Wu, J. Zong, X. Xie, W. Chen, Z. Sun, D. Shen, S. Wang, Y. Zhang, M. Zhang, X. Wang, F. Song, H. Zhang, and B. Wang, “Searching the $\text{Mn}(\text{Sb},\text{Bi})_2\text{Te}_4$ family of materials for the ideal intrinsic magnetic topological insulator,” arXiv e-prints , arXiv:1903.09934 (2019), [arXiv:1903.09934 \[cond-mat.mtrl-sci\]](#).
- [68] Y. Deng, Y. Yu, M. Zhu Shi, J. Wang, X. H. Chen, and Y. Zhang, “Magnetic-field-induced quantized anomalous Hall effect in intrinsic magnetic topological insulator MnBi_2Te_4 ,” arXiv e-prints , arXiv:1904.11468 (2019), [arXiv:1904.11468 \[cond-mat.mtrl-sci\]](#).
- [69] C. Liu, Y. Wang, H. Li, Y. Wu, Y. Li, J. Li, K. He, Y. Xu, J. Zhang, and Y. Wang, “Quantum phase transition from axion insulator to Chern insulator in MnBi_2Te_4 ,” arXiv e-prints , arXiv:1905.00715 (2019), [arXiv:1905.00715 \[cond-mat.mes-hall\]](#).
- [70] J. Ge, Y. Liu, J. Li, H. Li, T. Luo, Y. Wu, Y. Xu, and J. Wang, “High-Chern-Number and High-Temperature Quantum Hall Effect without Landau Levels,” arXiv e-prints , arXiv:1907.09947 (2019), [arXiv:1907.09947 \[cond-mat.mes-hall\]](#).
- [71] Y.-J. Hao, P. Liu, Y. Feng, X.-M. Ma, E. F. Schwier, M. Arita, S. Kumar, C. Hu, R. Lu, M. Zeng, Y. Wang, Z. Hao, H. Sun, K. Zhang, J. Mei, N. Ni, L. Wu, K. Shimada, C. Chen, Q. Liu, and C. Liu, “Gapless surface Dirac cone in antiferromagnetic topological insulator MnBi_2Te_4 ,” arXiv e-prints , arXiv:1907.03722 (2019), [arXiv:1907.03722 \[cond-mat.mtrl-sci\]](#).
- [72] Y. J. Chen, L. X. Xu, J. H. Li, Y. W. Li, C. F. Zhang, H. Li, Y. Wu, A. J. Liang, C. Chen, S. W. Jung, C. Cacho, H. Y. Wang, Y. H. Mao, S. Liu, M. X. Wang, Y. F. Guo, Y. Xu, Z. K. Liu, L. X. Yang, and Y. L. Chen, “Topological Electronic Structure and Its Temperature Evolution in Antiferromagnetic Topological Insulator MnBi_2Te_4 ,” arXiv e-prints , arXiv:1907.05119 (2019), [arXiv:1907.05119 \[cond-mat.mtrl-sci\]](#).
- [73] H. Li, S.-Y. Gao, S.-F. Duan, Y.-F. Xu, K.-J. Zhu, S.-J. Tian, W.-H. Fan, Z.-C. Rao, J.-R. Huang, J.-J. Li, Z.-T. Liu, W.-L. Liu, Y.-B. Huang, Y.-L. Li, Y. Liu, G.-B. Zhang, H.-C. Lei, Y.-G. Shi, W.-T. Zhang, H.-M. Weng, T. Qian, and H. Ding, “Dirac surface states in intrinsic magnetic topological insulators EuSn_2As_2 and MnBi_2Te_4 ,” arXiv e-prints , arXiv:1907.06491 (2019), [arXiv:1907.06491 \[cond-mat.mtrl-sci\]](#).
- [74] P. Swatek, Y. Wu, L.-L. Wang, K. Lee, B. Schunk, J. Yan, and A. Kaminski, “Gapless Dirac surface states in the antiferromagnetic topological insulator MnBi_2Te_4 ,” arXiv e-prints , arXiv:1907.09596 (2019), [arXiv:1907.09596 \[cond-mat.mtrl-sci\]](#).
- [75] R. Li, J. Wang, X.-L. Qi, and S.-C. Zhang, “Dynamical axion field in topological magnetic insulators,” *Nature Phys.* **6**, 284 (2010).
- [76] J. Wang, R. Li, S.-C. Zhang, and X.-L. Qi, “Topological magnetic insulators with corundum structure,” *Phys. Rev. Lett.* **106**, 126403 (2011).
- [77] J. Wang, B. Lian, and S.-C. Zhang, “Dynamical axion field in a magnetic topological insulator superlattice,” *Phys. Rev. B* **93**, 045115 (2016).
- [78] P. Rani, A. Saxena, R. Sultana, V. Nagpal, S. S. Islam, S. Patnaik, and V. P. S. Awana, “Crystal Growth and basic transport and magnetic properties of MnBi_2Te_4 ,” arXiv e-prints , arXiv:1906.09038 (2019), [arXiv:1906.09038 \[cond-mat.mtrl-sci\]](#).
- [79] See Supplemental Material for details.
- [80] N. Read and D. Green, “Paired states of fermions in two dimensions with breaking of parity and time-reversal symmetries and the fractional quantum hall effect,” *Phys. Rev. B* **61**, 10267–10297 (2000).
- [81] X.-L. Qi, T. L. Hughes, and S.-C. Zhang, “Chiral topological superconductor from the quantum hall state,” *Phys. Rev. B* **82**, 184516 (2010).
- [82] J. Wang, Q. Zhou, B. Lian, and S.-C. Zhang, “Chiral topological superconductor and half-integer conductance plateau from quantum anomalous hall plateau transition,” *Phys. Rev. B* **92**, 064520 (2015).
- [83] Q. L. He, L. Pan, A. L. Stern, E. C. Burks, X. Che, G. Yin, J. Wang, B. Lian, Q. Zhou, E. S. Choi, K. Murata, X. Kou, Z. Chen, T. Nie, Q. Shao, Y. Fan, S.-C. Zhang, K. Liu, J. Xia, and K. L. Wang, “Chiral majorana fermion modes in a quantum anomalous hall in-

- ulator–superconductor structure,” *Science* **357**, 294–299 (2017).
- [84] G. E. Volovik, “Graphite, graphene, and the flat band superconductivity,” *JETP Letters* **107**, 516–517 (2018).
- [85] F. Wu, A. H. MacDonald, and I. Martin, “Theory of phonon-mediated superconductivity in twisted bilayer graphene,” *Phys. Rev. Lett.* **121**, 257001 (2018).
- [86] B. Lian, Z. Wang, and B. A. Bernevig, “Twisted bilayer graphene: A phonon-driven superconductor,” *Phys. Rev. Lett.* **122**, 257002 (2019).
- [87] Y. W. Choi and H. J. Choi, “Strong electron-phonon coupling, electron-hole asymmetry, and nonadiabaticity in magic-angle twisted bilayer graphene,” *Phys. Rev. B* **98**, 241412 (2018).
- [88] J. Zhang, D. Wang, M. Shi, T. Zhu, H. Zhang, and J. Wang, “Dynamical magnetoelectric effect in antiferromagnetic insulator $\text{Mn}_2\text{Bi}_2\text{Te}_5$,” arXiv e-prints, arXiv:1906.07891 (2019), [arXiv:1906.07891 \[cond-mat.mes-hall\]](#).
- [89] J. Wu, F. Liu, M. Sasase, K. Ienaga, Y. Obata, R. Yukawa, K. Horiba, H. Kumigashira, S. Okuma, T. Inoshita, and H. Hosono, “Natural van der Waals Heterostructures with Tunable Magnetic and Topological States,” arXiv e-prints, arXiv:1905.02385 (2019), [arXiv:1905.02385 \[cond-mat.mtrl-sci\]](#).
- [90] A. Alexandradinata, X. Dai, and B. A. Bernevig, “Wilson-loop characterization of inversion-symmetric topological insulators,” *Phys. Rev. B* **89**, 155114 (2014).
- [91] D. J. Thouless, M. Kohmoto, M. P. Nightingale, and M. den Nijs, “Quantized hall conductance in a two-dimensional periodic potential,” *Phys. Rev. Lett.* **49**, 405–408 (1982).

SUPPLEMENTARY MATERIAL FOR ”FLAT CHERN BAND FROM TWISTED BILAYER MnBi_2Te_4 ”

THE CONTINUUM MODEL OF TBMBT AND PARAMETERS, BAND STRUCTURE CALCULATION

In this section, we give the interlayer hopping Hamiltonian of the continuum model of tBMBT, and list the parameters for FM and AFM phases we fitted from the first-principles calculations [60]. More details of the continuum model is given in Sec. .

The interlayer Moiré hopping potential $T(\mathbf{r})$ is as shown in the main text Eq. (5). Except for the zero Fourier component T_0 , we have kept the lowest six nonzero Fourier components of the Moiré potential at momenta

$$\begin{aligned} \mathbf{g}_1 &= k_m(1, 0), & \mathbf{g}_2 &= k_m(1/2, \sqrt{3}/2), & \mathbf{g}_3 &= k_m(-1/2, \sqrt{3}/2), \\ \mathbf{g}_4 &= k_m(-1, 0), & \mathbf{g}_5 &= k_m(-1/2, -\sqrt{3}/2), & \mathbf{g}_6 &= k_m(1/2, -\sqrt{3}/2), \end{aligned} \quad (9)$$

where $k_m = 8\pi \sin(\theta/2)/\sqrt{3}a_0$ is the length of the Moiré reciprocal vector. Higher Fourier components are expected to decay exponentially with the Fourier momentum [32], therefore can be ignored.

For FM phase tBMBT, the interlayer hopping matrices can be divided into a nonmagnetic part and an FM part, namely, $T_j = T_j^N + \gamma_f T_j^{\text{FM}}$ ($0 \leq j \leq 6$). The dimensionless parameter γ_f is so chosen that $\gamma_f = 1$ corresponds to the phase transition point of an untwisted FM bilayer MnBi_2Te_4 from trivial insulator to a Chern insulator of Chern number 1. The zero Fourier component matrices T_0^N and T_0^{FM} have the form

$$T_0^N = \begin{pmatrix} t_1 & -i\lambda & & \\ & t_2 & i\lambda & \\ -i\lambda & & t_2 & \\ & i\lambda & & t_1 \end{pmatrix}, \quad T_0^{\text{FM}} = \begin{pmatrix} u_1 & -i\kappa & & \\ & -u_2 & -i\kappa & \\ -i\kappa & & u_2 & \\ & -i\kappa & & -u_1 \end{pmatrix}, \quad (10)$$

while the nonzero Fourier component matrices T_j^N and T_j^{FM}

$$T_j^N = \begin{pmatrix} \omega_j t'_1 & -i\lambda' & & \\ & t'_2 & i\lambda' & \\ -i\lambda' & & t'_2 & \\ & i\lambda' & & \omega_j t'_1 \end{pmatrix}, \quad T_j^{\text{FM}} = \begin{pmatrix} \omega_j u'_1 & -i\kappa' & & \\ & -u'_2 & -i\kappa' & \\ -i\kappa' & & u'_2 & \\ & -i\kappa' & & -\omega_j u'_1 \end{pmatrix}, \quad (1 \leq j \leq 6) \quad (11)$$

where $\omega_j = e^{i(-1)^j \frac{2\pi}{3}}$ is the phase factor due to the relative in-plane shift between the closest Bi atoms of the two SLs.

In the AFM phase tBMBT, the interlayer hopping matrices T_j take the form $T_j = T_j^N$ as allowed by symmetries, where T_j^N are still given by Eqs. (10) and (11). The derivation of these matrices can be found in Sec. .

The parameters of the monolayer Hamiltonian in the main text Eqs. (3) and (4), and the interlayer hopping parameters in Eqs. (10) and (11) for the FM and the AFM phases tBMBT are listed in Tab. I, which are estimated from the first-principles calculations (see Secs. and).

tBMBT parameters	FM phase	AFM phase
γ (eV·Å ²)	12.8	17.0
m_0 (eV)	-0.0863	-0.132
β_0 (eV·Å ²)	6.72	9.40
α (eV·Å)	1.85	3.20
m_1 (eV)	-0.176	0.05
β_1 (eV·Å ²)	8.68	
m_2 (eV)	-0.0116	0.12
β_2 (eV·Å ²)	6.49	
α' (eV·Å)	-0.532	
t_1 (eV)	-0.0202	-0.0444
t'_1 (eV)	0.00086	0.00073
t_2 (eV)	0.0160	0.0386
t'_2 (eV)	0.00025	0.0011
λ (eV)	0.0470	0.0530
λ' (eV)	0.0010	0.0020
u_1 (eV)	-0.0068	
u'_1 (eV)	-0.00002	
u_2 (eV)	0.0053	
u'_2 (eV)	-0.0015	
κ (eV)	0.0101	
κ' (eV)	0.00339	

TABLE I. Parameters for the tBMBT continuum model in the FM phase and the AFM phase.

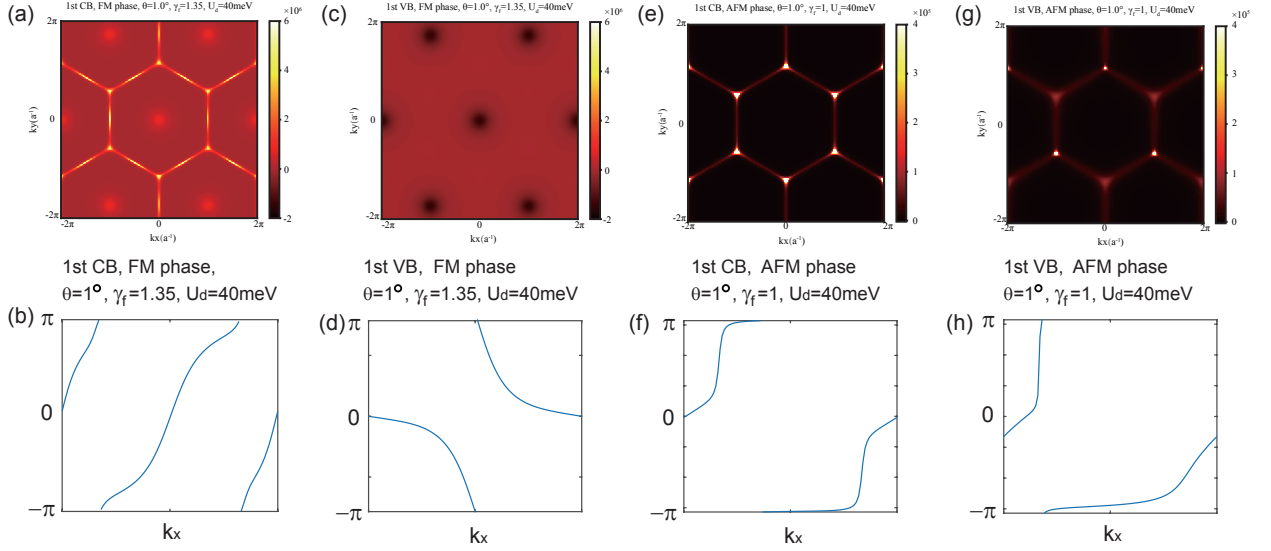


FIG. 4. The Berry curvature and Wilson loop eigenvalue for the 1st conduction band and the 1st valence band, where the parameters are (a)-(d) FM phase, $\theta = 1^\circ$, $U_d = 40\text{meV}$, $\gamma_f = 1.02$ (band structure given in main text Fig. 2(b)), and (e)-(h) AFM phase, $\theta = 1^\circ$, $\gamma_{af} = 0.75$, $U_d = 40\text{meV}$ (band structure given in main text Fig. 3(b)).

The band structure is calculated by Fourier transforming the continuum model in main text Eq. (1) into the momentum space [32]. The transformation brings the Hamiltonian into a momentum space hopping model

$$H_{\mathbf{Q}\mathbf{Q}'}(\mathbf{k}) = \begin{pmatrix} h_{1,\frac{\theta}{2}}(\mathbf{k} + \mathbf{Q}) + U_d & T_0 \\ T_0^\dagger & h_{2,-\frac{\theta}{2}}(\mathbf{k} + \mathbf{Q}) - U_d \end{pmatrix} \delta_{\mathbf{Q},\mathbf{Q}'} + \left[\sum_{j=1}^6 \begin{pmatrix} 0 & T_j \\ 0 & 0 \end{pmatrix} \delta_{\mathbf{Q},\mathbf{Q}'+\mathbf{g}_j} + h.c. \right], \quad (12)$$

where $\mathbf{Q} = m_1\mathbf{g}_1 + m_2\mathbf{g}_2$ ($m_1, m_2 \in \mathbb{Z}$) runs over all reciprocal lattice sites, and \mathbf{k} is in the Moiré BZ. To do numerical calculations, one can take a cutoff in reciprocal lattice \mathbf{Q} . We note that the form of the monolayer $\mathbf{k} \cdot \mathbf{p}$ Hamiltonian $h_{l,\frac{\theta}{2}}(\mathbf{k})$ given in the main text is only valid for small \mathbf{k} . At large \mathbf{k} , the dispersions of $h_{l,\frac{\theta}{2}}(\mathbf{k})$ may severely deviate from the actual monolayer band structure and incorrectly disperse into the CNP gap, which will affect the low energy

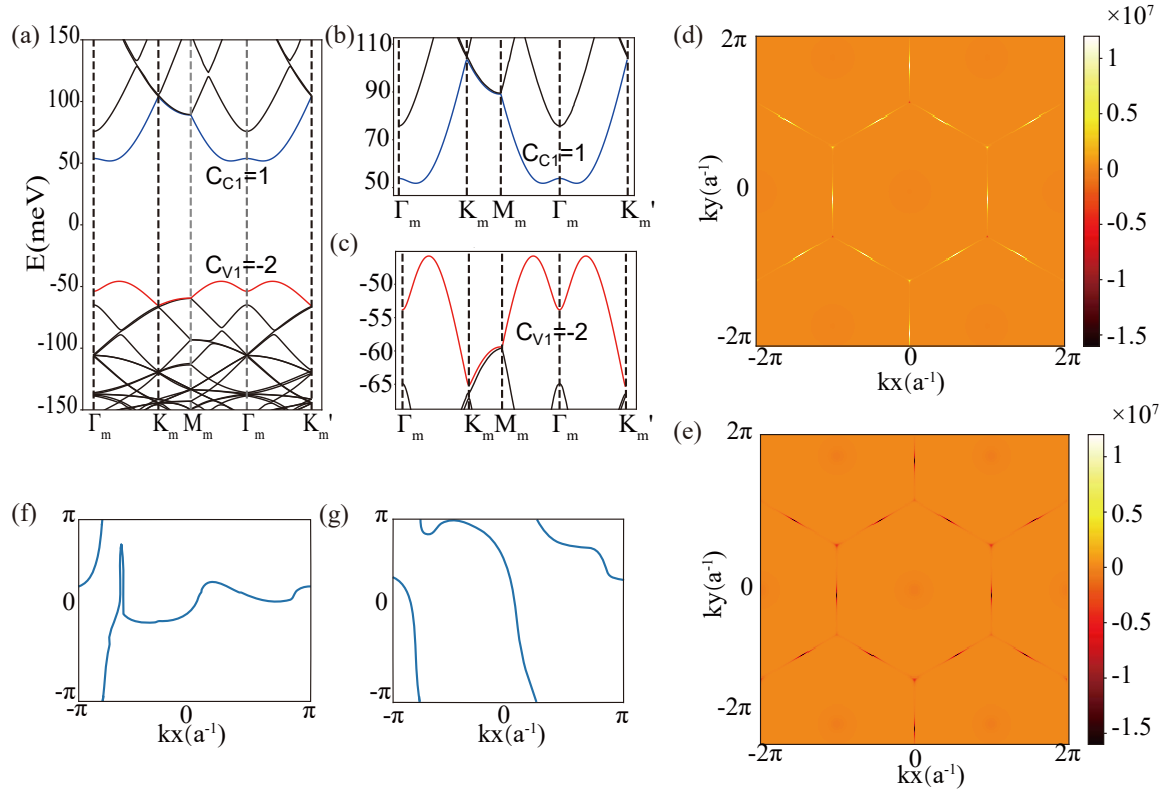


FIG. 5. The band structure, Berry curvature and Wilson loop eigenvalue for the 1st conduction band and the 1st valence band of AFM phase with the parameters $\theta = 2^\circ$, $U_d = 40\text{meV}$, $\gamma_{af} = 1.35$. (a) The band structure. (b)-(c) Zoom in plot of (a) showing the bandwidth of the 1st conduction band and 1st valence band. (d)-(e) The Berry curvature for the 1st conduction band and the 1st valence band. (f)-(g) The Wilson loop eigenvalue for the 1st conduction band and the 1st valence band.

band structure. To avoid this, one can either take a small enough cutoff in \mathbf{Q} so that large \mathbf{k} is not involved, or correct the large \mathbf{k} dispersions by adding proper higher power terms of \mathbf{k} in $h_{l,\frac{\theta}{2}}(\mathbf{k})$. The low energy physics is not affected by the \mathbf{Q} cutoff or large \mathbf{k} dispersion corrections.

The Chern numbers of the bands can be calculated by either the Wilson loop winding number [90] or the integration of Berry curvature [91] in the Moiré BZ. Figs. 4 shows two examples for the band structures of main text Fig. 2(b) and Fig. 3(b), respectively, where we have plotted the Berry curvature in the Moiré BZ and the Wilson loop eigenvalues sweeping across the Moiré BZ for the 1st conduction band and 1st valence band. The Chern number is simply equal the the Wilson loop winding number. Fig. 5 shows another example in the AFM phase at larger angle $\theta = 2^\circ$, where the first valence band carries Chern number -2 .

THE 3D BULK MnBi_2Te_4 MODEL

The form and parameters of our tBMBT model for two SLs of MnBi_2Te_4 is derived from the reduction of the 3D bulk MnBi_2Te_4 model into two-dimensional SLs, which we briefly review and describe in this section.

MnBi_2Te_4 has a seven layer structure (Te-Bi-Te-Mn-Te-Bi-Te), which gives a septuple layer (SL). Each atomic layer forms a triangular lattice, while each SL forms an ABCABCA stacking (from the bottom layer to the top layer). The in-plane lattice constant is $a_0 = 4.334\text{\AA}$, and the z direction thickness of each unit cell (which consists of 3 SLs) is $c_0 = 40.91\text{\AA}$.

Here we present two kinds of crystal structures: (1) the ground state structure which has the SLs forming AB stacking, namely, the stacking of the atomic layers is ABCABCA-BCABCAB-CABCABC-.... (2) the unstable structure where SLs form AA stacking, namely, atomic layer stacking ABCABCA-ABCABCA-....

In both AB stacking and AA stacking, the generic nonmagnetic 3D bulk MnBi_2Te_4 has an effective $\mathbf{k} \cdot \mathbf{p}$ Hamiltonian

for momentum \mathbf{k} measured from the Γ point [60]:

$$H_N(\mathbf{k}) = E_0(\mathbf{k})\mathbf{1}_4 + \begin{pmatrix} M(\mathbf{k}) & A_2k_- & A_1k_z & \\ A_2k_+ & -M(\mathbf{k}) & & -A_1k_z \\ A_1k_z & & -M(\mathbf{k}) & A_2k_- \\ & -A_1k_z & A_2k_+ & M(\mathbf{k}) \end{pmatrix}, \quad (13)$$

where $\mathbf{1}_4$ is the 4×4 identity matrix, $E_0(\mathbf{k}) = C + D_1k_z^2 + D_2(k_x^2 + k_y^2)$, $M(\mathbf{k}) = M_0 + B_1k_z^2 + B_2(k_x^2 + k_y^2)$, and $k_{\pm} = k_x \pm ik_y$. The basis of the Hamiltonian is given by

$$\Psi_{\Gamma} = (|p_{z,\text{Bi}}^+, \uparrow\rangle, |p_{z,\text{Te}}^-, \downarrow\rangle, |p_{z,\text{Te}}^-, \uparrow\rangle, |p_{z,\text{Bi}}^+, \downarrow\rangle)^T,$$

where $|p_{z,\text{Bi}}^+, s_z\rangle$ is the bonding state of p_z orbitals of the two Bi layers in a unit cell with spin $s_z = \uparrow, \downarrow$, and $|p_{z,\text{Te}}^-, s_z\rangle$ is the anti-bonding state of p_z orbitals of the top and bottom Te layers in a unit cell with spin s_z . The symmetries of the 3D nonmagnetic phase are the time reversal T , the inversion P , the 3-fold rotation about z axis C_{3z} and the 2-fold rotation about x axis C_{2x} . Their symmetry operations are given by $TH_N(\mathbf{k})T^{-1} = U_T H_N^*(-\mathbf{k})U_T^{\dagger}$, $PH_N(\mathbf{k})P^{-1} = U_P H_N(-\mathbf{k})U_P^{\dagger}$, $C_{3z}H_N(\mathbf{k})C_{3z}^{-1} = U_{C_{3z}} H_N(C_{3z}\mathbf{k})U_{C_{3z}}^{\dagger}$ and $C_{2x}H_N(\mathbf{k})C_{2x}^{-1} = U_{C_{2x}} H_N(C_{2x}\mathbf{k})U_{C_{2x}}^{\dagger}$, where

$$U_T = \begin{pmatrix} & & -1 \\ & 1 & \\ -1 & & \\ 1 & & \end{pmatrix}, U_P = \begin{pmatrix} 1 & & & \\ & -1 & & \\ & & -1 & \\ & & & 1 \end{pmatrix}, U_{C_{3z}} = \begin{pmatrix} e^{\frac{i\pi}{3}} & & & \\ & e^{-\frac{i\pi}{3}} & & \\ & & e^{\frac{i\pi}{3}} & \\ & & & e^{-\frac{i\pi}{3}} \end{pmatrix}, U_{C_{2x}} = \begin{pmatrix} & & i \\ & & -i \\ -i & & \\ i & & \end{pmatrix}, \quad (14)$$

respectively.

The layered structure of MnBi_2Te_4 makes the bands less dispersive in the k_z direction. To approximately recover the real space layered structure in the z direction, we can apply the substitution

$$k_z \rightarrow \frac{1}{c_0} \sin(k_z c_0), \quad k_z^2 \rightarrow \frac{2}{c_0^2} [1 - \cos(k_z c_0)] \quad (15)$$

in the $\mathbf{k} \cdot \mathbf{p}$ Hamiltonian $H_N(\mathbf{k})$. In this way, we have a Hamiltonian periodic in k_z , i.e., $H_N(\mathbf{k}) = H_N(\mathbf{k} + \frac{2\pi}{c_0}\hat{z})$, and we can extract out the Hamiltonian within each SL and the hoppings between neighbouring SLs. We shall apply this substitution in the following.

At low temperatures, either ferromagnetism (FM) or anti-ferromagnetism (AFM) is developed in MnBi_2Te_4 . In the below, we describe their effective models, respectively.

(1) **The FM phase.** In this phase, the system develops a uniform FM order in the z direction. When the FM order is in the $+z$ direction, the 3D $\mathbf{k} \cdot \mathbf{p}$ Hamiltonian at Γ point becomes $H_{\text{FM}}(\mathbf{k}) = H_N(\mathbf{k}) + H_{\text{FM}}(\mathbf{k})$, where

$$H_{\text{FM}}(\mathbf{k}) = \begin{pmatrix} M_1(\mathbf{k}) & A_4k_- & A_3k_z & \\ A_4k_+ & -M_2(\mathbf{k}) & & A_3k_z \\ A_3k_z & & M_2(\mathbf{k}) & -A_4k_- \\ & A_3k_z & -A_4k_+ & -M_1(\mathbf{k}) \end{pmatrix}. \quad (16)$$

Here we have defined $M_1(\mathbf{k}) = M_1 + B_3k_z^2 + B_4(k_x^2 + k_y^2)$, and $M_2(\mathbf{k}) = M_2 + B_5k_z^2 + B_6(k_x^2 + k_y^2)$. If the FM order is in the $-z$ direction, H_{FM} flips its sign. Similarly, we apply the substitution (15) to obtain the layered Hamiltonian of the FM phase.

(2) **The AFM phase.** In this case, the system develops a FM order in the $\pm z$ direction in each SL, while two neighbouring SLs have opposite FM orders. Accordingly, the unit cell is doubled in the z direction, and the Brillouin zone (BZ) is reduced by 1/2 in the k_z direction.

The AFM order yields an AFM term in the l_z -th SL to be in the following form:

$$H_{\text{AFM}}(\mathbf{k}_{\parallel}, l_z) = (-1)^{l_z} \begin{pmatrix} M_1 & & & \\ & -M_2 & & \\ & & M_2 & \\ & & & -M_1 \end{pmatrix}, \quad (17)$$

where M_1 and M_2 are exchange fields, and we have ignored the \mathbf{k} dependence of the AFM term (which is difficult to obtain accurately from first-principles). The full Hamiltonian of the AFM phase is given by $H_{\text{AFM}} = H_N + H_{\text{AFM}}$.

The AFM term H_{AFM} induces a hopping between 3D momenta \mathbf{k} and $\mathbf{k} + \frac{\pi}{c_0} \hat{\mathbf{z}}$. This opens two gaps of approximate magnitudes $2M_1$ and $2M_2$ at $k_z = \pm \frac{\pi}{2c_0}$, and reduces the BZ size by one half in the k_z direction.

The parameters for the AA stacking and AB stacking 3D MnBi_2Te_4 in the FM and AFM phases can be determined from first-principles calculations [60].

THE CONTINUUM MODEL OF TWISTED BILAYER MnBi_2Te_4

In this section, we obtain the single particle continuum model for the twisted bilayer MnBi_2Te_4 (tBMBT) Moiré pattern from the $\mathbf{k} \cdot \mathbf{p}$ Hamiltonian of the 3D MnBi_2Te_4 in Sec. . Hereafter we use $\mathbf{k} = (k_x, k_y)$ to denote the 2D momentum.

Using substitution (15), we can separate the 3D $\mathbf{k} \cdot \mathbf{p}$ Hamiltonian into the monolayer Hamiltonian in each SL and the z direction hopping terms between neighboring SLs. The monolayer Hamiltonian of the l 's layer ($l = 1, 2$) takes the form $h_l(\mathbf{k}) = h_{\text{N}}(\mathbf{k}) + \gamma_f h_{\text{FM}}(\mathbf{k})$ for FM state, and $h_l(\mathbf{k}) = h_{\text{N}}(\mathbf{k}) - \gamma_{af} (-1)^l h_{\text{AFM}}(\mathbf{k})$, where γ_f and γ_{af} are two dimensionless parameters for tuning the strength of the FM and AFM orders, respectively, while $h_{\text{FM}}(\mathbf{k})$ and $h_{\text{AFM}}(\mathbf{k})$ are fixed. Since the definitions of γ_f and γ_{af} are up to a rescaling, we need to fix a reference point for them. For the FM phase, we fix $\gamma_f = 1$ to be the critical point for an untwisted bilayer MnBi_2Te_4 to undergo the transition from a trivial insulator (where $\gamma_f < 1$) to a Chern insulator of Chern number 1 (where $\gamma_f > 1$). With this choice of reference point, we find the FM order strength given by our first-principles calculations for 3D bulk MnBi_2Te_4 corresponds to $\gamma_f = \gamma_{f0} = 0.75$. The realistic FM order strength may differ from the value given by first-principles calculations, and is tunable by a small external magnetic field. For the AFM phase, we simply fix $\gamma_{af} = 1$ to be the AFM strength obtained from our first-principles calculations.

The normal term is given by

$$h_{\text{N}}(\mathbf{k}) = \epsilon_0(\mathbf{k}) \mathbf{1}_4 + \begin{pmatrix} m(\mathbf{k}) & \alpha k_- & & \\ \alpha k_+ & -m(\mathbf{k}) & & \\ & & -m(\mathbf{k}) & \alpha k_- \\ & & \alpha k_+ & m(\mathbf{k}) \end{pmatrix}, \quad (18)$$

where $\epsilon_0(\mathbf{k}) = \epsilon_0 + \gamma \mathbf{k}^2$, and $m(\mathbf{k}) = m_0 + \beta_0 \mathbf{k}^2$. The parameters obtained in this way are related to the 3D bulk parameters in Sec. (for a particular stacking structure) by $\epsilon_0 = C + \frac{2D_1}{c_0^2}$, $\gamma = D_2$, $m_0 = M_0 + \frac{2B_1}{c_0^2}$, $\beta_0 = B_2$, and $\alpha = A_2$. Since ϵ_0 is a constant term, we can set $\epsilon_0 = 0$ by redefining the zero point of energy, so we have $\epsilon_0(\mathbf{k}) = \gamma \mathbf{k}^2$.

The FM term is given by

$$h_{\text{FM}}(\mathbf{k}) = \begin{pmatrix} m_1(\mathbf{k}) & \alpha' k_- & & \\ \alpha' k_+ & -m_2(\mathbf{k}) & & \\ & & m_2(\mathbf{k}) & -\alpha' k_- \\ & & -\alpha' k_+ & -m_1(\mathbf{k}) \end{pmatrix}, \quad (19)$$

where $m_1(\mathbf{k}) = m_1 + \beta_1 \mathbf{k}^2$, and $m_2(\mathbf{k}) = m_2 + \beta_2 \mathbf{k}^2$. The parameters are approximately $m_1 = \gamma_{f0}^{-1}(M_1 + \frac{2B_3}{c_0^2})$, $m_2 = \gamma_{f0}^{-1}(M_2 + \frac{2B_5}{c_0^2})$, $\beta_1 = \gamma_{f0}^{-1}B_4$, $\beta_2 = \gamma_{f0}^{-1}B_6$, and $\alpha' = \gamma_{f0}^{-1}A_4$, where $\gamma_{f0} = 0.75$ is the dimensionless parameter characterizing the FM order strength of the 3D first-principles result we defined earlier.

The AFM term is given by

$$h_{\text{AFM}}(\mathbf{k}) = \begin{pmatrix} m_1 & & & \\ & -m_2 & & \\ & & m_2 & \\ & & & -m_1 \end{pmatrix}, \quad (20)$$

where m_1 and m_2 are constants. In this case, one has $m_1 = M_1$, and $m_2 = M_2$ (since $\gamma_{af} = 1$ is fixed to be the AFM order strength given by our 3D first-principles calculations). Besides, one could find out the interlayer hopping matrix for both the AA stacking and the AB stacking configuration.

In the tBMBT, there are both AA stacking positions and AB/BA stacking positions. As a commonly used approximation, we can assume the monolayer Hamiltonian is only a function of momentum $-i\nabla$ and is independent of positions, but is rotated by angle $\pm\theta/2$ in the first and second layers, respectively. Namely, $h_{l,\pm\theta/2}(\mathbf{k}) = R_{\pm\frac{\theta}{2}}^\dagger h_l(\mathbf{k}) R_{\pm\frac{\theta}{2}}$, where $R_{\pm\frac{\theta}{2}} = \text{diag}(e^{\pm i\theta/4}, e^{\mp i\theta/4}, e^{\mp i\theta/4}, e^{\pm i\theta/4})$ is the rotation matrix. We estimate the parameters of the tBMBT monolayer Hamiltonian by properly averaging between the AB stacking and AA stacking parameters.

Meanwhile, the interlayer hopping is a function of position \mathbf{r} , with a spatial period given by the Moire superlattice. Keeping the lowest six nonzero Fourier components, we can write the interlayer Moiré hopping potential $T(\mathbf{r})$ from layer 2 to layer 1 in the form

$$T(\mathbf{r}) = T_0 + \sum_{j=1}^6 T_j e^{i\mathbf{g}_j \cdot \mathbf{r}}, \quad (21)$$

where T_0 and T_j ($1 \leq j \leq 6$) are 4×4 hopping matrices, and \mathbf{g}_j ($1 \leq j \leq 6$) are the six smallest Moiré reciprocal vectors in Eq. (9). We assume $\mathbf{r} = 0$ corresponds to AA stacking. In this convention, the AB stacking positions \mathbf{r}_{AB} satisfy $e^{i\mathbf{g}_j \cdot \mathbf{r}_{AB}} = e^{-i(-1)^j \frac{2\pi}{3}}$. From the substitution (15), we find the hopping matrices for the FM phase with FM order strength γ_f are of the form

$$T_0 = \begin{pmatrix} t_1 + \gamma_f u_1 & 0 & -i(\lambda + \gamma_f \kappa) & 0 \\ 0 & t_2 - \gamma_f u_2 & 0 & i(\lambda - \gamma_f \kappa) \\ -i(\lambda + \gamma_f \kappa) & 0 & t_2 + \gamma_f u_2 & 0 \\ 0 & i(\lambda - \gamma_f \kappa) & 0 & t_1 - \gamma_f u_1 \end{pmatrix}, \quad (22)$$

$$T_j = \begin{pmatrix} (t'_1 + \gamma_f u'_1)\omega_j & 0 & -i(\lambda' + \gamma_f \kappa') & 0 \\ 0 & t'_2 - \gamma_f u'_2 & 0 & i(\lambda' - \gamma_f \kappa') \\ -i(\lambda' + \gamma_f \kappa') & 0 & t'_2 + \gamma_f u'_2 & 0 \\ 0 & i(\lambda' - \gamma_f \kappa') & 0 & (t'_1 - \gamma_f u'_1)\omega_j \end{pmatrix},$$

where $\omega_j = e^{i(-1)^j \frac{2\pi}{3}}$. They can then be decomposed into the nonmagnetic part and FM part (if FM phase) as shown in Eqs. (10) and (11). For the AFM phase, the hopping matrices are given by setting $u_j = u'_j = \kappa = \kappa' = 0$ in Eq. (22). The factor ω_j is the phase factor due to the relative in-plane shift between closest Bi atoms in neighboring SLs (assume the hopping is dominantly between the closest atoms). This is because at AA stackings, the closest Bi atoms of the orbital $|p_{z,\text{Bi}}, s\rangle$ in the two SLs are not on top of each other but shifted in-plane by $1/3$ unit cell, while at AB stackings, the closest Bi atoms in the two SLs are on top of each other. In contrast, the closest Te atoms in AA stacking are on top of each other, while shifted in-plane by $1/3$ unit cell at AB stacking.

The coefficient can be determined by let $T(\mathbf{r})$ at AA stacking ($\mathbf{r} = 0$) and AB stacking ($e^{i\mathbf{g}_j \cdot \mathbf{r}} = \omega_j^{-1}$) positions agree with that of untwisted AA stacking and untwisted AB stacking structures, respectively (which is a good approximation for small twist angle [32]). For the FM phase, they are roughly related to the 3D parameters by

$$\begin{aligned} t_1 - 3t'_1 &= -\frac{2(B_1 + D_1)|_{AA}}{c_0^2}, & t_1 + 6t'_1 &= -\frac{2(B_1 + D_1)|_{AB}}{c_0^2}, & u_1 - 3u'_1 &= -\frac{2B_3|_{AA}}{\gamma_{f0}c_0^2}, & u_1 + 6u'_1 &= -\frac{2B_3|_{AB}}{\gamma_{f0}c_0^2}, \\ t_2 + 6t'_2 &= -\frac{2(D_1 - B_1)|_{AA}}{c_0^2}, & t_2 - 3t'_2 &= -\frac{2(D_1 - B_1)|_{AB}}{c_0^2}, & u_2 + 6u'_2 &= -\frac{2B_5|_{AA}}{\gamma_{f0}c_0^2}, & u_2 - 3u'_2 &= -\frac{2B_5|_{AB}}{\gamma_{f0}c_0^2}, \\ \lambda + 6\lambda' &= \frac{A_1|_{AA}}{c_0}, & \lambda - 3\lambda' &= \frac{A_1|_{AB}}{c_0}, & \kappa + 6\kappa' &= \frac{A_3|_{AA}}{\gamma_{f0}c_0}, & \kappa - 3\kappa' &= \frac{A_3|_{AB}}{\gamma_{f0}c_0}, \end{aligned} \quad (23)$$

where $\gamma_{f0} = 0.75$ is the FM strength corresponding to the 3D bulk first-principles result. For the AFM phase, $u_j = u'_j = \kappa = \kappa' = 0$, while the other parameters are given by Eq. (23). The continuum model Hamiltonian of tBMBT can then be written as

$$H = \begin{pmatrix} h_{1,\theta/2}(-i\nabla) & T(\mathbf{r}) \\ T^\dagger(\mathbf{r}) & h_{2,-\theta/2}(-i\nabla) \end{pmatrix}, \quad (24)$$

as we have in the main text.

DISCUSSION ON THE FM AND AFM PHASES

Since the 3D MnBi_2Te_4 is in the AFM phase, it is more likely that the tBMBT ground state is AFM as well. In this case, it is expected that the AFM phase can be easily flipped into the FM phase by a magnetic field. In first principles calculations, the AFM and the FM phases of MnBi_2Te_4 have competing energies.

Experimentally, the AFM phase of MnBi_2Te_4 is shown to undergo a spin-flop transition into the FM phase around 3T [63, 68]. Theoretically, the AFM exchange interaction between neighboring SLs is estimated by ab initio calculations to be $J_\perp \approx -0.02 \text{ meV}/\mu_B^2$ [63], while the magnetic moment of Mn atom is $5\mu_B$. Therefore, the magnetic field for polarizing the system into the FM phase can be estimated to be $B_c \approx |J_\perp| \times 5\mu_B \approx 2\text{T}$. Therefore, we conclude that the AFM phase of tBMBT can be easily flipped into the FM phase by a magnetic field around $2 \sim 4\text{T}$.

In addition, it might also be possible to control the magnetization of tBMBT by adding top and bottom FM heterostructures, which may induce proximity exchange couplings. We leave the investigation of this possibility to the future studies.
